Atomic Three-Body Loss as a Dynamical Three-Body Interaction

A. J. Daley,[1] J. M. Taylor,[2] S. Diehl,[1] M. Baranov,[1] and P. Zoller[1]

[1]*Institute for Theoretical Physics, University of Innsbruck, A-6020 Innsbruck, Austria
and Institute for Quantum Optics and Quantum Information of the Austrian Academy of Sciences, A-6020 Innsbruck, Austria*
[2]*Department of Physics, Massachusetts Institute of Technology, Building 6C-411, Cambridge, Massachusetts 02139, USA*

We discuss how large three-body loss of atoms in an optical lattice can give rise to effective hard-core three-body interactions. For bosons, in addition to the usual atomic superfluid, a dimer superfluid can then be observed for attractive two-body interactions. The nonequilibrium dynamics of preparation and stability of these phases are studied in 1D by combining time-dependent density matrix renormalization group techniques with a quantum trajectories method.

　　　　　　　　　PACS numbers: 03.75.Lm, 42.50.−p

Cold atomic gases in optical lattices have proven a test bed for understanding novel quantum phases [1] and non-equilibrium many-body dynamics [2,3]. Recently, Syassen *et al.* [4] showed that a strong two-body loss process for molecules in an optical lattice [1] could produce an effective, elastic hard-core repulsion and thus a Tonks gas [4,5]. This is related to the quantum Zeno effect: a large loss dynamically suppresses processes creating two-body occupation on a particular site. Whilst elastic two-body interactions occur in many systems, regimes where elastic three-body interactions dominate are rare in nature. Here we discuss how the ubiquitous, though normally undesirable three-body losses of atomic physics experiments can induce effective three-body interactions. These are associated with interesting quantum phases, including Pfaffian states [6], and could be used to stabilize three-component Fermi mixtures [7], assisting in the production of a color superfluid state [8]. We investigate Bosons in an optical lattice, where a three-body hard-core constraint stabilizes the system with attractive two-body interactions, and a dimer superfluid phase emerges. We focus on the dynamics of this intrinsically time-dependent system, both testing the hard-core constraint for finite loss rates, and studying nonequilibrium properties including decay. In one dimension, the exact evolution is computed by combining time-dependent density matrix renormalization group methods (*t*-DMRG) [2,3] with a quantum trajectories approach from quantum optics [9].

Three-body recombination [10] in an optical lattice corresponds to decay into the continuum of unbound states, and thus loss from the lattice. This can be described by a master equation in the Markov approximation [9], which for atoms in the lowest band of an optical lattice can be projected onto the corresponding basis of Wannier functions [1,5], associated with bosonic annihilation operators b_i on site i. We can separate the master equation into terms which conserve particle number, corresponding to an effective Hamiltonian H_{eff}, and terms which remove three particles on a site:

$$\dot\rho^{(n)} = -i(H_{eff}\rho^{(n)} - \rho^{(n)}H_{eff}^\dagger) + \frac{\gamma_3}{12}\sum_i 2b_i^3\rho^{(n+3)}(b_i^\dagger)^3,$$

where $\rho^{(n)}$ denotes the system density operator with n atoms and $\hat n_i = b_i^\dagger b_i$. The dominant loss term is on-site three-body decay [11] and γ_3 is the corresponding rate. The effective Hamiltonian is

$$H_{eff} = H - i\frac{\gamma_3}{12}\sum_i (b_i^\dagger)^3 b_i^3, \qquad (1)$$

$$H = -J\sum_{\langle i,j\rangle} b_i^\dagger b_j + \frac{U}{2}\sum_i \hat n_i(\hat n_i - 1) + \sum_i \varepsilon_i \hat n_i, \qquad (2)$$

with J the nearest neighbor tunneling amplitude, U the elastic two-body interaction, and ε_i the local potential. The Hamiltonian is valid in the limit where J, ε_i, Un, $\ll \omega$ with ω the band gap and n the mean density. In an experiment these parameters, in particular U, may be tuned while γ_3 remains constant and large [12]. In Fig. 1(c) we show example values of γ_3, U, and J using numbers for Cesium as a function of lattice depth.

If we begin in a pure state with N particles, then loss processes lead to heating, in that they produce a mixed state of different particle numbers. Within a fixed particle number sector, the dynamics are described by H_{eff}. Three-body interactions emerge most clearly in the limit of rapid decay: $\gamma_3 \gg J, U, \epsilon_i$. If we define the projector P onto the subspace of states with at most two atoms per site and $Q = 1 - P$, then in second order perturbation theory we obtain the effective model

$$H_{eff}^P \approx PHP - \frac{2i}{\gamma_3}PHQHP = PHP - i\frac{6J^2}{\gamma_3}P\sum_j c_j^\dagger c_j P, \qquad (3)$$

where $c_j = (b_j^2/\sqrt2)\sum_{k\in N_j} b_k$, and N_j denotes the set of nearest neighbors of site j. The term PHP describes the Hubbard dynamics, Eq. (2), supplemented by the hard-core
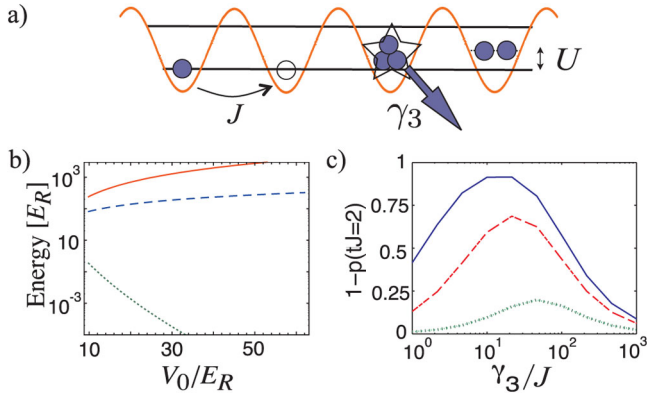
a)

FIG. 1 (color online). (a) Bosons in an optical lattice in the presence of three-body loss at a rate γ_3. (b) Example model parameters estimated for Cs at a magnetic field of 15 Gauss (where the scattering length is $20a_0$ and the recombination length $\sim 500a_0$ [10] where a_0 is the Bohr radius) as a function of lattice depth V_0, showing γ_3 (solid line), U (dashed), and J (dotted). Values of γ_3 are obtained by integrating the measured three-body recombination rates in free space over a state with three particles in a single Wannier function. (c) The probability that at least one loss event has occurred at time $tJ = 2$, beginning with a single particle on each of 10 sites, and $U/J = 3$ (solid line), 5 (dashed), and 10 (dotted), computed using t-DMRG methods (see text for details).

constraint $(b_i^\dagger)^3 = 0$. Furthermore, the effective loss rates decrease as J^2/γ_3 [13].

Thus, we see the clear emergence of a three-body hard-core constraint in the limit $\gamma_3/J \gg 1$. We can study the physics of the projected model PHP to obtain a qualitative understanding of the quantum phases associated with the projection. However, the residual loss processes make this system intrinsically time dependent, and can give rise to heating. We therefore study the full nonequilibrium dynamics, by combining t-DMRG methods [2,3] with an expression of the master equation as an average over *quantum trajectories* [9]. Each stochastic trajectory begins from an initial pure state (sampled from the initial density matrix), and can be interpreted as describing a single experimental run, in which losses occurred at particular times t_n and on sites i_n. The evolution is described by the non-Hermitian H_{eff}, except for times t_n, where losses (or *quantum jumps*) occur,

$$i\hbar \frac{d}{dt}|\psi(t)\rangle = H_{\mathrm{eff}}|\psi(t)\rangle; \qquad |\psi(t_n^+)\rangle = \frac{C_{i_n}|\psi(t_n)\rangle}{||C_{i_n}|\psi(t_n)\rangle||}, \tag{4}$$

where the jump operator $C_i = b_i^3$ corresponds to three-body loss on site i. In stochastic simulation of the master equation, the times t_n are points where the norm of the state falls below a randomly chosen threshold. At these times, a random jump operator is selected according to the probabilities $p_{i_n} \propto \langle \psi(t_n)|C_i^\dagger C_i|\psi(t_n)\rangle$ and applied. In this way we can both investigate individual trajectories and compute

expectation values from the master equation. The latter is performed by stochastic average over both initial states and over jump events, which converges rapidly as the number of trajectories is increased.

The need to simulate many trajectories for convergence is offset by the efficiency of simulating states rather than density matrices [14], and we can also make use of existing optimizations for conserved quantities. Despite the application of local jump operators, we find the evolution quite efficient, especially for small numbers of jumps [15].

As an example of the suppression of loss, we consider preparing a homogenous initial state at unit filling in a deep optical lattice where $U/J \to \infty$. At time $t = 0$ we suddenly ramp the lattice to a finite depth, and observe the probability p that a single three-body loss event has occurred as a function of time. In Fig. 1(c) we plot this probability for different U/J as a function of γ_3/J. We see a clear suppression of loss rates for large γ_3/J, and also a substantial decrease for larger U/J, resulting from the decreased amplitude for doubly occupied sites.

In the limit of large γ_3, it is instructive to study the equilibrium phase diagram of the projected Hamiltonian PHP. For $U/J > 0$, we observe the well-known Mott insulator (MI) and atomic superfluid phases of the Bose-Hubbard model. However, the three-body hard-core condition will also stabilize the system for $U/J < 0$, where we find a dimer superfluid phase [see Fig. 2(a)]. This is characterized by the vanishing of the order parameter signalling superfluidity of single atoms (ASF) ($\langle b_i \rangle = 0$), while a
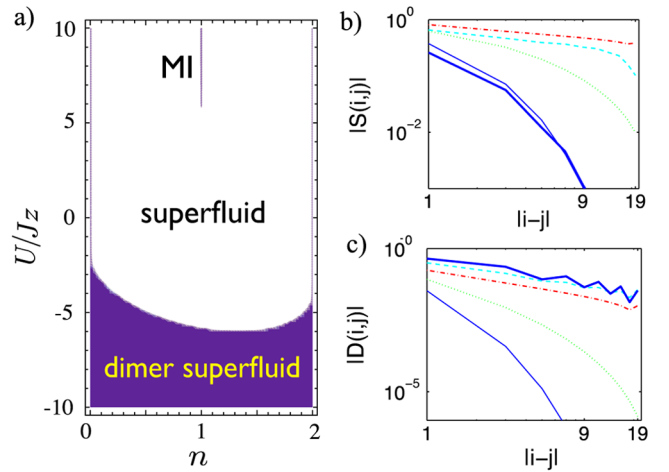

FIG. 2 (color online). Equilibrium analysis of the projected Bose-Hubbard model PHP. (a) Mean-field phase diagram as a function of $U/(Jz)$ and density, n. (b,c) Magnitude of off-diagonal elements of (b) the single particle density matrix $|S(i, j)| = |\langle b_i^\dagger b_j \rangle|$ and (c) the dimer density matrix, $|D(i, j)| = |\langle b_i^\dagger b_i^\dagger b_j b_j \rangle|$, as a function of $|i - j|$, for $U/J = 10$ (thin solid line), 5 (dotted), 0 (dot-dash), -5 (dashed), and -10 (thick solid line). These results are computed for 20 particles on 20 lattice sites in one dimension, with box boundary conditions and $i + j = 21$, using imaginary time evolution in t-DMRG, and plotted on a logarithmic scale.

dimer superfluidity (DSF) order parameter persists ($\langle b_i^2 \rangle \neq 0$). The superfluid regimes are connected via a quantum phase transition associated with the spontaneous breaking of a discrete Z_2 symmetry, reminiscent of an Ising transition [16]: the DSF order parameter transforms with the double phase $\sim \exp 2i\theta$ compared to the ASF order parameter $\sim \exp i\theta$. Consequently, the symmetry $\theta \rightarrow \theta + \pi$ exhibited by the DSF order parameter is broken when reaching the ASF phase.

We can obtain a qualitative mean-field picture using a homogeneous Gutzwiller ansatz wavefunction, given for the projected Hilbert space by $|\Psi\rangle = \prod_i |\Psi\rangle_i$, where $|\Psi\rangle_i = r_0 e^{i\phi_0} |0\rangle_i + r_1 e^{i\phi_1} |1\rangle_i + r_2 e^{i\phi_2} |2\rangle_i$. Normalization implies $\sum_\alpha r_\alpha^2 = 1$, while the filling is $n = r_1^2 + 2r_2^2 \leq 2$. To examine the phases, we find the energy $E/M^d = \langle\Psi|H|\Psi\rangle$, $E(r_\alpha, \phi_\alpha) = Ur_2^2 - Jzr_1^2[r_0^2 + 2\sqrt{2}r_2r_0\cos\Phi + 2r_2^2]$, where $\Phi = \phi_2 + \phi_0 - 2\phi_1$ and M^d is the number of lattice sites. For any r_α the energy is minimized for Φ an integer multiple of 2π. For $r_1, r_0 \neq 0$ placing us in the ASF phase with $|\langle b_i \rangle|^2 = r_1^2(r_0 + \sqrt{2}r_2)^2 \neq 0$, the phase-locking expression contributes a "source" term linear in r_2 to the energy, and consequently the minimum of the energy cannot be located at $r_2 = 0$. Thus, a finite atomic condensate always implies a dimer component $|\langle b_i^2 \rangle|^2 = 2(r_0 r_2)^2$, though the reverse is not true.

At fixed n, the energy is a function, e.g., of r_1 alone. For the second order transition found within our mean-field theory, an instability for atomic superfluidity is indicated by its mass term crossing zero, $\partial^2 E(r_1 = 0)/\partial r_1^2 \equiv 0$. This leads to a critical interaction strength for the ASF-DSF transition, $U_c/(Jz) = -2[1 + n/2 + 2\sqrt{n(1 - n/2)}]$. Within the DSF phase the order parameter obeys $|\langle b_i^2 \rangle|^2 = n(1 - n/2)$ independent of the interaction strength. For $n \rightarrow 2$, we approach a MI state in a second order transition. At $n = 1$ we find that the ASF-DSF transition takes place at the same coupling strength as the ASF-MI transition, but with the opposite sign. The complete mean-field phase diagram in the plane of density and interaction strength is plotted in Fig. 2(a).

From the last term in Eq. (3), we can estimate the initial loss rate from the ground state Gutzwiller wave function. We obtain the rate $\gamma_{\rm eff} = 3J^2z/\gamma_3M^d(\langle\hat{n}_i^2\rangle - n) \times (n + |\langle b_i \rangle|^2)$, which is zero in the MI, and $\propto n^2$ for the DSF, $\gamma_{\rm eff} = 3J^2zM^dn^2/\gamma_3$. In the DSF phase, the critical temperature $T_c \propto n^{2/3}$ at low densities, and the energy density deposited by a single loss, $\Delta E_{\rm loss} = (z + 1)|U|n/(2M^d)$. The number of independent loss events needed to melt the DSF is then proportional to $T_c/\Delta E_{\rm loss}$, and the melting time strongly decreases for increasing density, proportional to $\gamma_3/[|U|(z + 1)J^2zn^{7/3}]$.

These qualitative features are reproduced in one dimension, as supported by numerical calculation of the ground state for PHP. In Figs. 2(b) and 2(c) we show the characterisation of the crossover between the ASF and DSF regimes in one dimension via the off-diagonal elements of the single particle density matrix, $S(i, j) = \langle b_i^\dagger b_j \rangle$, and

the dimer density matrix $D(i, j) = \langle b_i^\dagger b_i^\dagger b_j b_j \rangle$. In the MI regime, the off-diagonal elements of $S(i, j)$ and $D(i, j)$ decay exponentially. As we enter the superfluid regime, quasi-long-range order is visible in the polynomial decay (linear on the logarithmic scale). As U/J is made more negative, we see a return to exponential decay for the off-diagonal elements of $S(i, j)$, but the off-diagonal elements of $D(i, j)$ still decay polynomially and, indeed, increase in magnitude. This characterizes the DSF regime in one dimension. Here, the transition to the DSF and MI regimes occurs at much smaller $|U/J|$ than in higher dimensions, but these two transitions again occur at similar $|U/J|$ for $n = 1$.

A DSF could be prepared via an adiabatic ramp beginning from states with very small amplitude of three-body occupation. We study two such scenarios as illustrated in Fig. 3(a): (i) Beginning from a MI, and ramping from $U/J = 30$ to $U/J = -8$ to produce a DSF (which is intuitive, but associated with large probability of decay); or (ii) applying a superlattice and beginning from a MI with two particles per site in the lowest wells, then switching the interaction rapidly to $U/J = -8$ on a time scale much faster than tunneling between the lowest wells and ramping down the superlattice. In each case, we compute dynamics for $\gamma_3/J = 250$, ramping parameters sufficiently
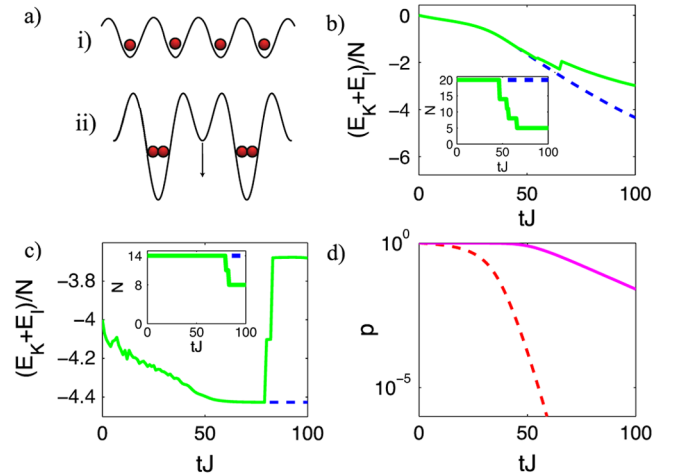

FIG. 3 (color online). Dynamics of adiabatic ramps into a dimer superfluid regime. (a) We begin with (i) a Mott-insulator state (ramping U/J), and (ii) a state with preprepared dimers in a superlattice (removing the superlattice). (b)-(c) The sum of kinetic (E_K) and interaction (E_I) energy and (inset) particle number as a function of time for two example trajectories, one with no loss events (dashed lines) and one with several loss events (solid lines). Here, (b) shows a ramp from $U/J = 30$ to $U/J = -8$, with $U(t) = \alpha J/(100 + 3tJ) + \gamma$, with α and γ ramp parameters, and (c) shows a ramp with a superlattice potential, $\varepsilon_l = V_0 \cos(2\pi l/3)$, where $V_0 \approx 30J \exp(-0.1tJ)$, adjusted so that $V_0(tJ = 100) = 0$, with fixed $U/J = -8$. In each case, $\gamma_3 = 250J$. For (b), we use 20 atoms on 20 lattice sites, for (c), 14 atoms on 23 lattice sites. (d) Plot showing the probability that no loss event has occurred after time t for the ramps in (b) (dashed line) and (c) (solid).
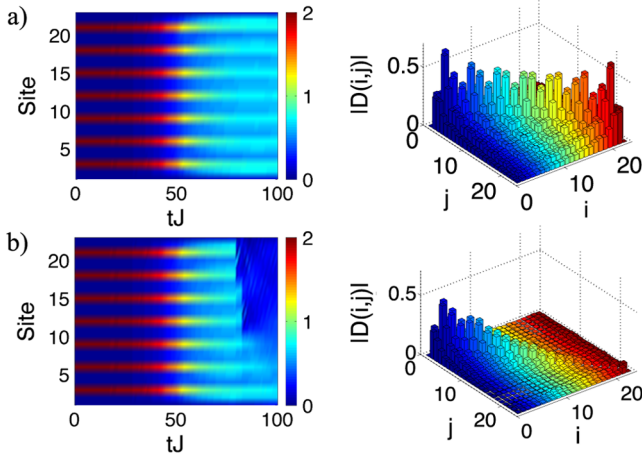
FIG. 4 (color online). Comparison of (a) lossless and (b) lossy trajectories from Fig. 3(c). We show the mean density $\langle n_i \rangle$ as a function of position and time, and magnitude of the dimer correlation function $|D(i, j)|$ $(i \neq j)$ at the end of the ramp.

slowly that without loss, the ground state will be reached with minimal presence of excited states.

In Figs. 3(b) and 3(c) we show the time dependence of the sum of kinetic and interaction energies, and of the total particle number, for example, trajectories. For each ramp type, we choose a "lossless" trajectory, where the ground state is reached adiabatically, and a "lossy" trajectory, where three-body loss events lead to heating of the system (as holes are produced that correspond to excited states).

In Fig. 3(d), we compare the probability for each type of ramp of producing the lossless trajectory. We see that for the ramp from the MI state, where we pass through a region of small U/J, the probability of such a trajectory is essentially zero. For the superlattice ramp, on the other hand, it is much more likely that we will obtain the ground state from a randomly chosen trajectory. This is because the superlattice both allows us to use large $|U/J|$, and facilitates the choice of a lower density.

In Fig. 4 we show the local density as a function of time and the final dimer density matrix $D(i, j)$ for (a) the lossless and (b) the lossy trajectories of Fig. 3(c). When a loss occurs it affects not just the density for the site on which it occurs, but also on neighboring sites due to the knowledge that we obtain of the position of the remaining particles. We also see clearly the destruction of correlations in the region of the system where the loss occurs. Note, however, that a single loss event does not always destroy the properties of the final state, and while the probability of an individual loss event increases with system size, a single loss event will change the character of the final state less.

The three-body interactions discussed here could have applications to producing Pfaffian-like states and stabilizing three-component mixtures. The theoretical approach we have used, quantum trajectories combined with t-DMRG, could also be applied to other classes of master

equations. Open questions regarding the nature of the ASF-DSF phase transition will be addressed within a quantum field theoretical treatment [17].

[1] I. Bloch, J. Dalibard, and W. Zwerger, Rev. Mod. Phys. **80**, 885 (2008).
[2] G. Vidal, Phys. Rev. Lett. **93**, 040502 (2004); F. Verstraete, V. Murg, and J. I. Cirac, Adv. Phys. **57**, 143 (2008).
[3] A. J. Daley et al., J. Stat. Mech. 04 (2004) P04005; S. R. White and A. E. Feiguin, Phys. Rev. Lett. **93**, 076401 (2004); F. Verstraete, J. J. Garcia-Ripoll, and J. I. Cirac, ibid. **93**, 207204 (2004).
[4] N. Syassen et al., Science **320**, 1329 (2008).
[5] J. J. Garcia-Ripoll et al., arXiv:0809.3679v1.
[6] B. Paredes, T. Keilmann, and J. I. Cirac, Phys. Rev. A **75**, 053611 (2007).
[7] T. B. Ottenstein et al., arXiv:0806.0587v2.
[8] A. Rapp, G. Zarand, C. Honerkamp, and W. Hofstetter, Phys. Rev. Lett. **98**, 160405 (2007).
[9] H. J. Carmichael, An Open Systems Approach to Quantum Optics (Springer, Berlin, 1993); C. W. Gardiner and P. Zoller, Quantum Noise (Springer, Berlin, 2005).
[10] See, e.g., T. Kraemer et al., Nature (London) **440**, 315 (2006).
[11] Off-site loss terms can arise from nonzero overlap of the corresponding Wannier functions, in analogy to off-site elastic interactions, which are discussed in L.-M. Duan, Europhys. Lett. **81**, 20001 (2008). These are small for γ_3 values used here.
[12] This is because nonuniversal behavior (where $\gamma_3 \not\propto a^4$, with a the scattering length) is observed away from a Feshbach resonance, where the rate of three-body recombination is large and weakly dependent on a [10], while the two-body scattering length a can be very small $(U \propto a)$.
[13] Note that off-site processes can place an upper bound on the useful value of γ_3, as increasing γ_3 suppresses on-site loss, but increases the rate of loss from processes involving neighboring lattice sites.
[14] M. Zwolak and G. Vidal, Phys. Rev. Lett. **93**, 207205 (2004); F. Verstraete, J. J. Garcia-Ripoll, and J. I. Cirac, Phys. Rev. Lett. **93**, 207204 (2004).
[15] We typically take the number of states retained in bipartite splittings [2], $\chi = 200$ in the results presented here.
[16] M. W. J. Romans, R. A. Duine, Subir Sachdev, and H. T. C. Stoof, Phys. Rev. Lett. **93**, 020405 (2004); L. Radzihovsky, J. I. Park, and P. B. Weichman, ibid. **92**, 160402 (2004); L. Radzihovsky, P. B. Weichman, and J. I. Park, Ann. Phys. (Leipzig) **323**, 2376 (2008).
[17] S. Diehl et al., (to be published).